

# Strong Precipitation Suppression by Aerosols in Marine Low Clouds

Chongxing Fan<sup>1,4</sup>, Minghuai Wang<sup>1</sup>, Daniel Rosenfeld<sup>2</sup>, Yannian Zhu<sup>3</sup>, Jihu Liu<sup>1</sup>, and Baojun Chen<sup>1</sup>

<sup>1</sup>School of Atmospheric Sciences & Joint International Research Laboratory of Atmospheric and Earth System Sciences, Nanjing University, China.

<sup>2</sup>Institute of Earth Sciences, The Hebrew University of Jerusalem, Jerusalem 91904, Israel.

<sup>3</sup>Meteorological Institute of Shaanxi Province, Xi'an, China.

<sup>4</sup>Department of Climate and Space Sciences and Engineering, University of Michigan, Ann Arbor, USA

Corresponding author: Minghuai Wang ([minghuai.wang@nju.edu.cn](mailto:minghuai.wang@nju.edu.cn)) and Daniel Rosenfeld ([daniel.rosenfeld@mail.huji.ac.il](mailto:daniel.rosenfeld@mail.huji.ac.il))

## Key Points:

- Precipitation is strongly suppressed with increasing cloud drop concentration.
- Sorting data by cloud thickness and using alternative CCN proxy rather than AOD are critical for studying aerosol-cloud interactions.
- Detectable rain initiates when the drop effective radius at the cloud top exceeds 14  $\mu\text{m}$ .

This is the author manuscript accepted for publication and has undergone full peer review but has not been through the copyediting, typesetting, pagination and proofreading process, which may lead to differences between this version and the [Version of Record](#). Please cite this article as doi: [10.1029/2019GL086207](https://doi.org/10.1029/2019GL086207)

## Abstract

The adjustment of cloud amount to aerosol effects occurs to a large extent in response to the aerosol effect on precipitation. Here the marine boundary layer clouds were studied by analyzing the dependence of rain intensity measured by Global Precipitation Measurement (GPM), on cloud properties. We showed that detectable rain initiates when the drop effective radius at the cloud top ( $r_e$ ) exceeds 14  $\mu\text{m}$ , and precipitation is strongly suppressed with increasing cloud drop concentration ( $N_d$ ), which contributes to the strong dependence of cloud amount on aerosols. The rainrate increases sharply with cloud thickness (CGT) and  $r_e$  when  $r_e > 14 \mu\text{m}$ . The dependence of rainrate on  $r_e$  and CGT presents a simple framework for precipitation susceptibility to aerosols, which explains other previously observed relationships. We showed that sorting data by CGT and using alternative cloud condensation nuclei (CCN) proxy rather than aerosol optical depth (AOD) are critical for studying aerosol-cloud-precipitation interactions.

## Plain Language Summary

Aerosol-cloud interaction remains the greatest uncertainty in future climate projection. Precipitation is a key process that mediates how the cloud amount responds to aerosol perturbations. Here we combined precipitation measured by the radar onboard the satellite of Global Precipitation Measurement (GPM) and cloud properties retrieved from Moderate Resolution Imaging Spectroradiometer (MODIS) onboard Aqua satellite for studying the dependence of rain intensity on cloud properties for marine boundary layer water clouds over the Southern Hemisphere Ocean. Our results showed that rain is sharply intensified when droplets at the cloud top grow larger than 14  $\mu\text{m}$ , and precipitation decreases with increasing cloud drop number concentration ( $N_d$ ). A simple framework to explain the relationship between precipitation and aerosols is proposed here by showing the dependence of precipitation on  $N_d$  and cloud geometric thickness. We also discussed why using aerosol optical depth (AOD) as CCN proxy in previous studies could lead to great uncertainties and why sorting cloud geometrical thickness is necessary.

## 1 Introduction

Aerosol particles, serving as cloud condensation nuclei (CCN), alter cloud physical and optical properties and therefore have important climate impact. However, climatic forcing caused by aerosol-cloud interaction remains the greatest uncertainty in climate forcing assessment (Boucher et al., 2013; Fan et al., 2016; Tao et al., 2012). This large uncertainty is often dominated by uncertainty in changes in cloud water amount or liquid water path caused by anthropogenic aerosol perturbation (Ackerman et al., 2004; Malavelle et al., 2017; Rosenfeld et al., 2019; Toll et al., 2019; Wang et al., 2012). Additional aerosols increase cloud droplet number concentration ( $N_d$ ) (Twomey, 1977), suppress precipitation and increase cloud amount (Albrecht, 1989), due to smaller cloud droplet radius and lower coalescence efficiency. Therefore, precipitation plays a key role in mediating cloud water response to aerosol perturbations.

As marine boundary layer clouds (MBLC) cover approximately one-third of the global oceans and make a significant contribution to global energy balance (Stephens & Slingo, 1992), this study focuses on aerosol effects on precipitation in MBLCs. How aerosols affect precipitation in MBLCs remains uncertain, partly because of difficulties to disentangle meteorological effects and to retrieve aerosol optical properties near clouds in satellite observations. A recent study found a positive relationship between precipitation rate (R) and

aerosol optical depth (AOD), with R derived from Tropical Rainfall Measurement Mission (TRMM) and AOD derived from Moderate Resolution Imaging Spectroradiometer (MODIS) observations (Koren et al., 2014). An aerosol invigoration effect was therefore proposed under a pristine marine environment with support from cloud-resolving model simulation, i.e., increasing aerosols in a pristine environment increases droplet mobility and condensation efficiency (G. Dagan et al., 2015; Guy Dagan et al., 2017; Fan et al., 2016; Koren et al., 2014, 2015).

In most previous satellite studies, aerosol optical depth (AOD) was widely employed to serve as a proxy for CCN concentration. However, AOD has been proven to have many drawbacks (Rosenfeld et al., 2016). Some disadvantages include weak relationships between AOD (or aerosol index, AI) and CCN (Kapustin et al., 2006; Stier, 2016), influence on AOD retrieval from clouds, and other meteorological effects (Boucher & Quaas, 2013; Gryspeerdt et al., 2016; Quan et al., 2018). By using updraft speed ( $W_b$ ) normalized  $N_d$  ( $N_d/W_b^{0.5}$ ) as CCN proxy rather than AOD (Rosenfeld et al., 2016), a recent study (Rosenfeld et al., 2019) addressed this challenge and found that aerosols explain about 3/4 of the variability in cloud radiative cooling effects when meteorological variables are fixed. By fixing cloud geometrical thickness (CGT), which encapsulates a large portion of meteorological effects, cloud fraction (CF) and cloud radiative effects are found to increase monotonically with increasing  $N_d$  (Rosenfeld et al., 2019). They hypothesized that CCN effects on CF are mediated by aerosols' control on coalescence and precipitation, which breaks up the clouds and depletes liquid water path (LWP). However, aerosol effects on precipitation were not examined in Rosenfeld et al. (2019).

Here we aim to use more direct precipitation estimates to examine the relationships between precipitation and CCN. Global Precipitation Measurement (GPM) Dual-frequency Precipitation Radar (DPR) dataset, which now is one of the most advanced precipitation measurement instruments onboard satellites, is chosen to measure the precipitation rate. Our study focuses on analyzing the Southern Hemisphere Ocean ( $0^\circ$ - $40^\circ$ S) and long-term southern summer (Nov.-Feb.) satellite data from 2014 to 2017. By integrating several advanced methods to retrieve  $N_d$  and rain rate more accurately and to isolate the meteorological factors (see Data and Methodology), this study demonstrates strong precipitation suppression by aerosols in MBLC, which contributes significantly to the cloud cover enhancement with increasing aerosols.

## 2 Data and Methodology

Cloud properties were obtained from the MODIS MYD06 product (Platnick et al., 2015). The spatial region was constrained over the ocean from  $0^\circ \sim 40^\circ$ S (**Figure S1**), and the time span covered the Southern Summer from 2014 to 2017. To make use of the more advantageous methods, the processing of MODIS products was similar to Rosenfeld et al. (2019). Each MODIS granule was divided into 306 scenes of approximately a  $1^\circ \times 1^\circ$  grid. Scenes with  $r_e$  uncertainty at  $2.1 \mu\text{m}$  greater than 10%, solar zenith angle greater than 65 degrees, and multilayer clouds were rejected. As this study mainly focused on marine low warm clouds, samples whose cloud top temperature was greater than 273.15K and cloud geometrical thickness was less than 800m were selected. Following Zhu et al. (2018),  $r_e$  and  $N_d$  for each valid scene (about 1-degree box) are calculated using the brightest 10% clouds of the scene, because it corresponds to the convective cores which are closest to adiabatic, our assumption for  $N_d$  retrieval process. It has been shown to minimize the bias in broken clouds relative to full clouds to less than 5% (Zhu et al., 2018). Note that the brightest 10% clouds are only used for retrieving

$N_d$  and  $r_e$  for each valid scene, and all marine low warm clouds are included for our analysis of aerosol-cloud-precipitation interactions.

One important meteorological factor that needs to be specially treated in this study is cloud geometrical thickness (CGT). It is defined as the subtraction between cloud top height and cloud base height. Both heights were retrieved based on the assumptions of dry adiabatic lapse rate from the surface to cloud base, and moist adiabatic rate within the clouds. Liquid water path (LWP), cloud top temperature (CTT) and sea surface temperature (SST) were thus required. Both LWP and CTT come from MODIS, while daily mean SST data was provided by the National Oceanic and Atmospheric Administration (NOAA).

Global Precipitation Measurement (GPM) products were chosen as our source of precipitation estimates. The core satellite carries a Ku/Ka-band Dual-frequency Precipitation Radar (DPR), which provides global precipitation measurements with improved accuracy. Compared to the TRMM precipitation radar, the DPR is more capable of sensing light rain and snowfall. Verification results showed that GPM DPR products can serve as a reliable reference for the calibration of multi-satellite precipitation products (Khan et al., 2018). The product we used in our study was Level 2 DPR Ka&Ku single orbit rainfall estimates (2A-DPR), with a spatial resolution of  $5.2\text{km} \times 125\text{m}$  and temporal resolution of 16 orbits per day. Level-2 DPR algorithms produce radar-only derived meteorological quantities on an instantaneous field-of-view basis. The variable we used was *precipRateNearSurface* (Iguchi et al., 2010).

In order to create a comparison, the GPM DPR dataset was collocated to the MODIS product. As is seen in **Figure S2**, for each MODIS scene, the GPM DPR sample points whose timestamp was within  $\pm 1$  hour and latitude and longitude were within  $\pm 0.5^\circ$  (in order to match the  $1^\circ \times 1^\circ$  grid of MODIS scene) were collected from each MODIS scene (the geometrical center of each MODIS scene). Average, median, maximum and minimum rain rate of all GPM sample points within each MODIS scene which meet the criteria above were derived.

### 3 Results

Cloud Geometrical Thickness (CGT) is a dominant meteorological factor and encapsulates a large portion of meteorological effects (Rosenfeld et al., 2019). It is closely associated with cloud properties. With CGT explaining 36% of the variability in cloud radiative effects (CRE) (Rosenfeld et al., 2019), it is necessary to stratify by CGT so that CCN effects can be separated from meteorological effects.

The relationship between maximum/average rain rate and  $N_d$  with several CGT bins is then presented in **Figure 1**. Each bin contains a comparable amount of sample points (**Table 1**). Data from the three southern summers were chosen. The total amount of samples is approximately 20,000. After being binned by CGT, a sharply negative relationship between rain rate (R) and  $N_d$  is clearly seen (**Figure 1**). This indicates that aerosols strongly suppress the precipitation. Furthermore, when comparing trends of different colors, **Figure 1** shows that R increases with CGT. This demonstrates that deeper clouds are likely to precipitate more due to larger LWP and larger  $r_e$ .

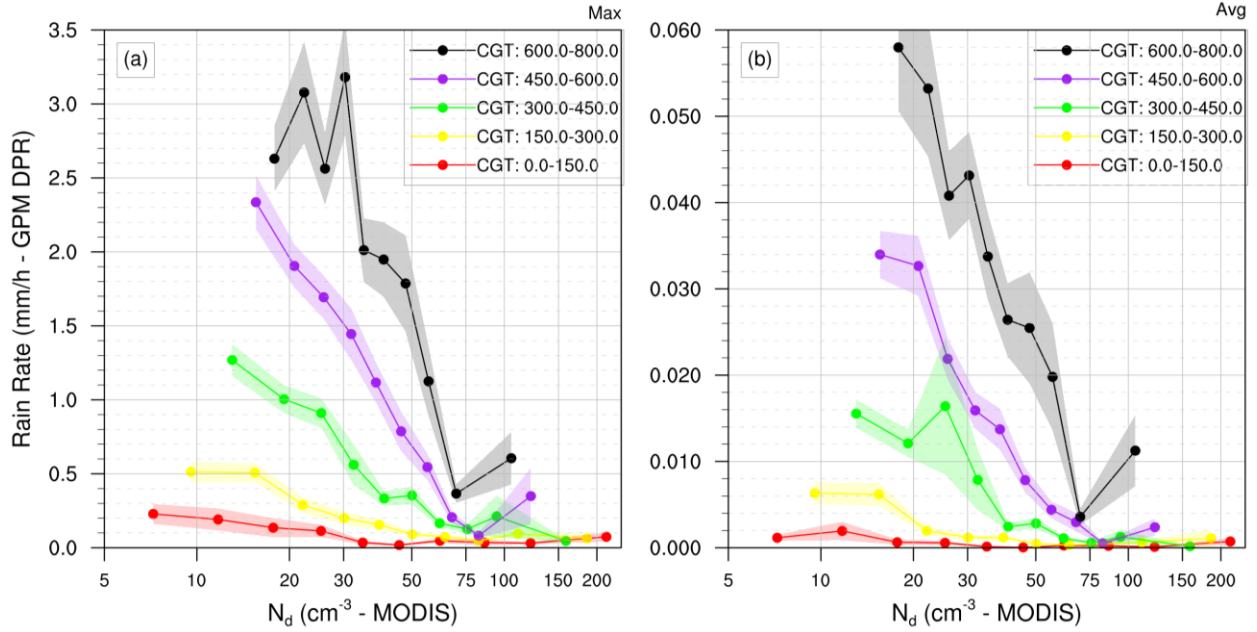


**Figure 1** Rain rate from GPM DPR as a function of MODIS cloud droplet concentration ( $N_d$ ) at constant CGT (m) bins. The left panel is the maximum rain rate while the right panel is the average rain rate. Each of the five colored trends corresponds to each CGT bin. The total number of valid sample points is 17,377. Shaded area indicates error range, calculated by standard deviation divided by the square root of the number of sample points.

**Table 1** The number of sample points in each bin drawn in **Figure 1**.

CGT Range (m)	Sample Count
0 – 150	1263
150 – 300	3850
300 – 450	5320
450 – 600	4623
600 – 800	2321

By using theoretical tools and measurements, it has been shown in previous studies that the coalescence rate has a tight relationship with cloud effective radius ( $r_e$ ) and will increase rapidly when  $r_e$  is greater than a certain threshold value (Chen et al., 2008; Freud & Rosenfeld, 2012; Pinsky & Khain, 2002; vanZanten et al., 2005). Here, we analyze the relationship between rain rate and  $r_e$  (**Figure 2**) and mark the threshold of  $r_e=14\mu\text{m}$  using a blue dashed line. Using advanced GPM DPR precipitation estimates, our results show a significant non-zero precipitation rate appears in both maximum and average rain rate when  $r_e \geq 14\mu\text{m}$ , especially for larger CGT bins, and negligible precipitation when  $r_e < 14\mu\text{m}$ . This clearly shows that the rain rate has a strong bond with the cloud effective radius, and detectable precipitation starts after  $r_e$  reaches a threshold of  $14\mu\text{m}$ . This is an independent result since the GPM DPR algorithm neither intakes

$r_e$  information from MODIS or other satellite instruments nor makes any assumption about  $r_e$  (Iguchi et al., 2010). An increase in  $N_d$  reduces cloud drop effective radius, and smaller droplet size dramatically suppresses the coalescence rate and thus the precipitation.

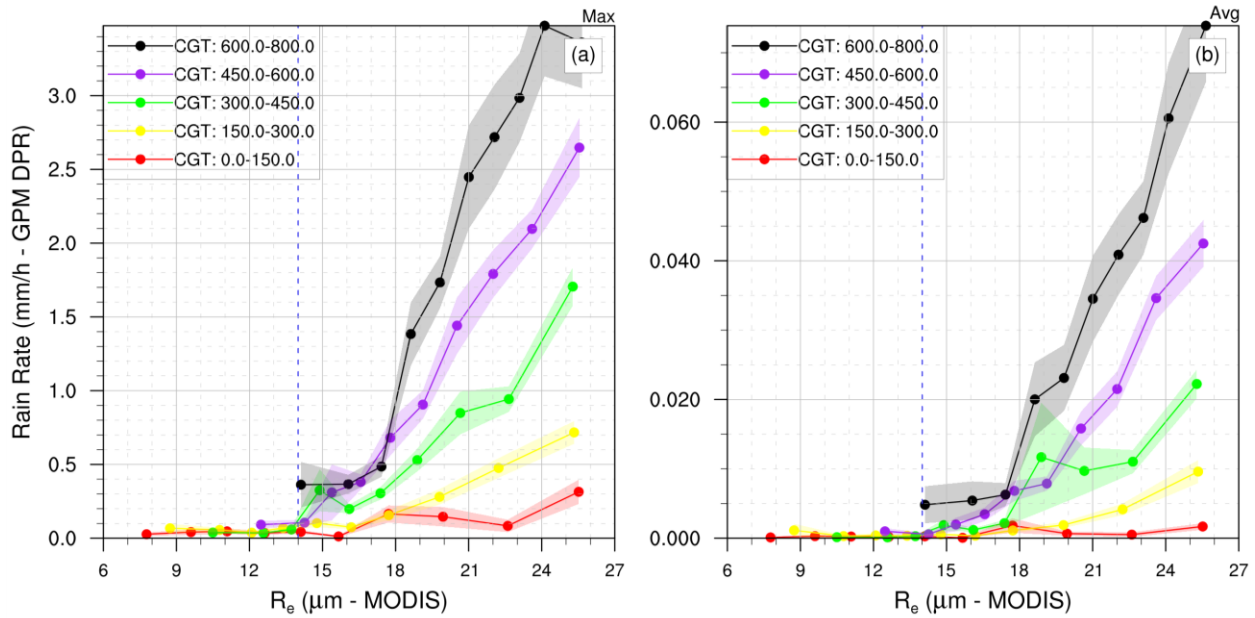


**Figure 2** Rain rate from GPM DPR as a function of the MODIS cloud top effective radius ( $r_e$ ) at constant CGT (m) bins. The left panel is the maximum rain rate, while the right panel is the average rain rate. The blue dash line refers to  $r_e=14\mu\text{m}$ . Each of the five colored lines corresponds to each CGT bin. The total number of valid sample points is 17,377. Shaded area indicates error range, calculated by standard deviation divided by the square root of the number of sample points.

Constraining meteorological factors and using alternative CCN proxies that are less affected by observational limitation and covariance factors allow us to provide a clear aerosol-cloud-precipitation relationship. To address the limitation of not sorting data with CGT bins and using AOD as CCN proxy, we plotted the relationships of between several variables and  $N_d$  without binning CGT, and also plotted the X-AOD relationship in accordance with the results in Koren et al. (2014) using the same data as in **Figure 2** and **Figure 1**.

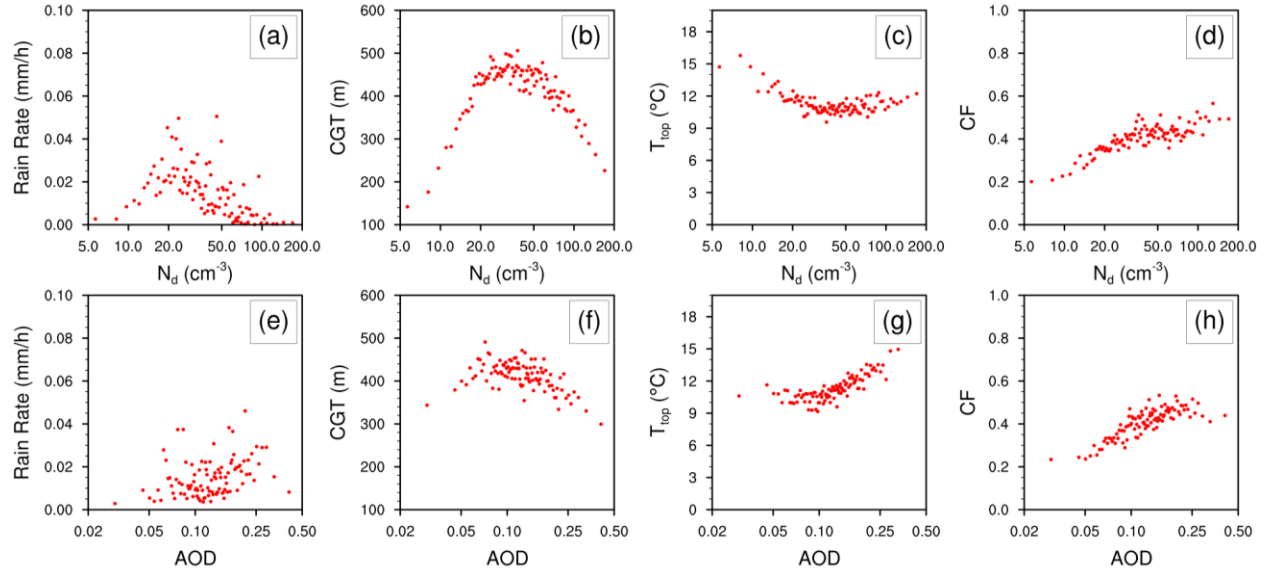


**Figure 3** Scatter plot showing the relationship of cloud/precipitation properties versus different CCN proxies **(a)** rain rate  $R$  versus cloud droplet number concentration  $N_d$ , **(b)** cloud geometrical height CGT versus  $N_d$ , **(c)** cloud top temperature  $T_{top}$  versus  $N_d$ , **(d)** cloud fraction CF versus  $N_d$ , **(e-h)** the same as (a-d) except the CCN proxy being AOD. All valid sample points are averaged to 100 points.

**Figure 3a** shows the first-increase-then-decrease trend of  $R$  with increasing  $N_d$ . The transitional point is approximately  $N_d \sim 20 \text{ cm}^{-3}$ . We now see the difference before and after CGT is binned, that is, meteorological factors are constrained. Without fixing CGT, a positive relationship between  $R$  and  $N_d$  is found when  $N_d < 20 \text{ cm}^{-3}$ , which is absent when data is sorted by CGT (**Figure 1a**). The positive relationship between  $R$  and  $N_d$  at low  $N_d$  partly comes from the dependence of CGT on  $N_d$ . **Figure 3b** and **Figure 3c** show that increasing  $N_d$  leads to larger CGT and higher cloud top with colder cloud top temperature ( $T_{top}$ ) when  $N_d < 20 \text{ cm}^{-3}$ . As deeper and thicker clouds generally produce more precipitation (**Figure 1a**), increasing  $N_d$  thus leads to larger  $R$  when  $N_d$  is low ( $< 20 \text{ cm}^{-3}$ ).

While CGT was shown to explain more than 60% of the variability in cloud radiative effects that are not explained by  $N_d$  (Rosenfeld et al., 2019), **Figure 3b** shows that CGT can be potentially affected by  $N_d$ , especially at low  $N_d$ . It has been hypothesized that the injection of aerosols on clouds in a very clean environment can trigger cloud growth (e.g., Koren et al., 2014; Christensen & Stephens, 2011; 2012). It, therefore, warrants further investigation in the future to develop better methods for meteorology classification at low  $N_d$ .

The difference between using  $N_d$  and AOD as CCN proxy is shown in **Figure 3**. When AOD is used as CCN proxy (**Figure 3e-h**), rain rate increases, cloud becomes first deeper and then shallower, cloud top temperature is warmer and cloud fraction increases with increasing AOD, which are consistent with previous studies and has been used to indicate the aerosol invigoration effect of marine low clouds (Koren et al., 2014). However, the trend of increasing rain rate largely disappears after  $N_d$  replaces AOD at large  $N_d$  (**Figure 3a-d**; **Figure 1**). Previous studies indicate that using AOD as CCN proxy could be problematic for studying aerosol-cloud-precipitation relationships, as this can be masked by meteorological covariance, observational limitation and poor relationship between CCN and AOD (Boucher & Quaas, 2013; Gryspeerdt et

al., 2016; Kapustin et al., 2006; Quan et al., 2018; Rosenfeld et al., 2016; Stier, 2016). The positive relationship between rain rate and AOD has been attributed to the covariation in AOD and rain rate caused by meteorological factors, especially wind speed (Nishant & Sherwood, 2017; Yang et al., 2016). Large wind speed usually leads to large AOD due to increasing sea salt aerosols with wind speed, while large wind speed also leads to a large rain rate as vigorous clouds are usually associated with stronger wind speed (Nishant & Sherwood, 2017). Our results here are consistent with the co-variation in AOD and rain rate caused by meteorological conditions, as  $N_d$  is mainly determined by accumulation mode particles and is less affected by wind speed in comparison to AOD. By using  $N_d$  as an alternate proxy we can avoid most of these drawbacks and obtain a clear aerosol-cloud-precipitation relationship. Note that  $N_d$  also depends on cloud processes other than CCN, such as cloud updraft speed, and a parameter that combines both  $N_d$  and updraft speed can serve as an even better CCN proxy (Rosenfeld et al., 2019).

#### 4 Conclusions

Aerosol-precipitation interaction, a fundamental process in aerosol-cloud interaction, was studied here by using advanced dual-frequency precipitation radar onboard GPM core satellite. With the aid of an improved algorithm to retrieve cloud and aerosol properties, a clear conceptual diagram for explaining aerosol-cloud-precipitation interactions emerged, as shown in **Figure 4**, which is extended from results in Rosenfeld et al. (2019). Precipitation generally increases with increasing CGT, because of the larger LWP and larger  $r_e$ . When CGT is fixed (along the X-axis), precipitation will monotonically decrease with increasing  $N_d$ , contributed mainly by suppression of precipitation from decreased droplet radius. A significant transition between heavy rain and light rain is evident when crossing the  $r_e=14\mu\text{m}$  line (yellow dash line). It is worth noting that larger  $N_d$  is needed to maintain  $r_e=14\mu\text{m}$  with larger CGT. Since  $LWP \propto CGT^2$ , more cloud water content in deeper clouds requires more  $N_d$  to consume the extra water (yellow dash line for  $r_e=14\mu\text{m}$  in **Figure 4**).

Our findings of precipitation suppression by aerosols support well the strong dependence of cloud fraction and cloud radiative effects (Rosenfeld et al., 2019). This precipitation suppression can only be revealed when we sort data by cloud geometrical thickness and use alternative CCN proxy rather than aerosol optical depth (AOD). Our results point to the critical role of precipitation in determining aerosol indirect effects. Precipitation processes and their interactions with aerosols in climate models are still not well represented, and improvement in their representation in climate models is critical for studying the effects of anthropogenic aerosols on climate change.



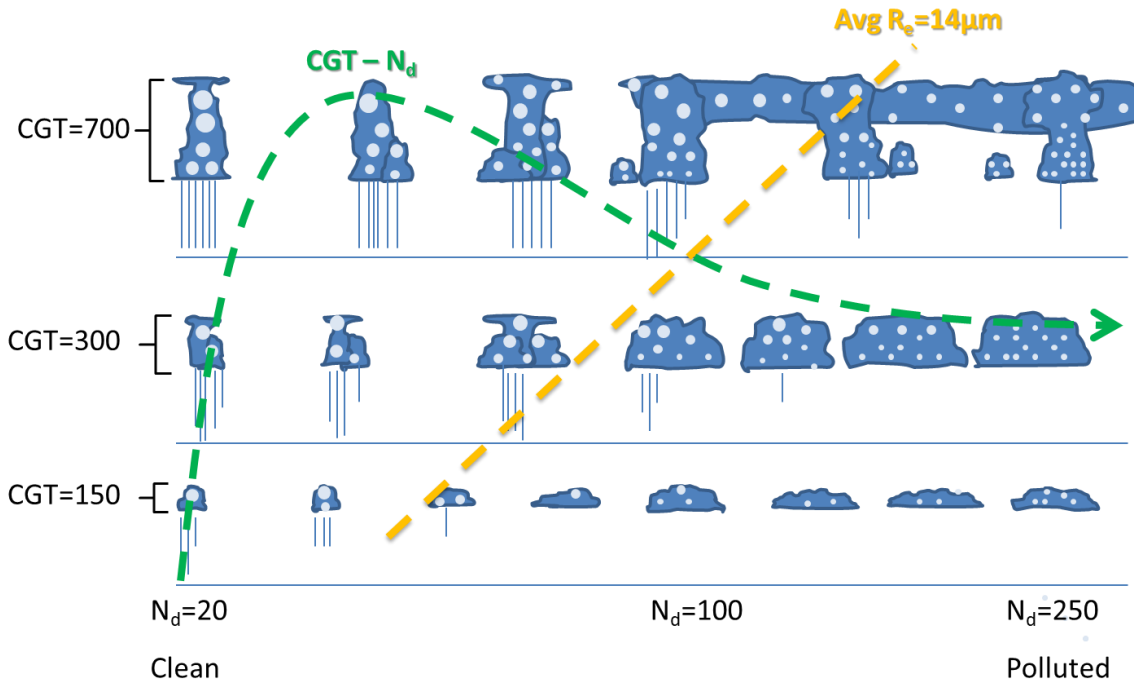


**Figure 4** Conceptual representation of the relationships between  $N_d$ , cloud properties and precipitation for marine boundary layer clouds of varying thicknesses, extended from Fig. 5 in Rosenfeld et al. (2019). Two main conclusions in this study are added into the diagram as two additional dashed lines. The yellow line indicates the average  $R_e=14\mu\text{m}$  line, and the green curve indicates the relationship between CGT and  $N_d$ . See the main text for further information.

### Acknowledgments

This research was supported by the Minister of Science and Technology of China (2017YFA0604002 and 2016YFC0200503) and by the Natural Science Foundation of China (91744208, 41925023, 41575073, 41621005 and 41575136). This research is also supported by the Collaborative Innovation Center of Climate Change, Jiangsu Province. The GPM 2ADPR and 3-IMERG data used in this study were retrieved from the NASA Precipitation Processing System (PPS) and cited in the references <https://pmm.nasa.gov/data-access/downloads/gpm>. The MODIS MYD06 Cloud data used in this study are publicly available in LAADS DAAC and cited in the references <https://modis.gsfc.nasa.gov/data/dataproduct/mod06.php>.

Author contributions: M.W. and D. R. designed this study; C. F., J. L., and Y. Z. acquired and processed data, and carried out the analysis. C. F., M. W., and D. R. interpreted data and wrote the manuscript. All authors contributed to the discussion.

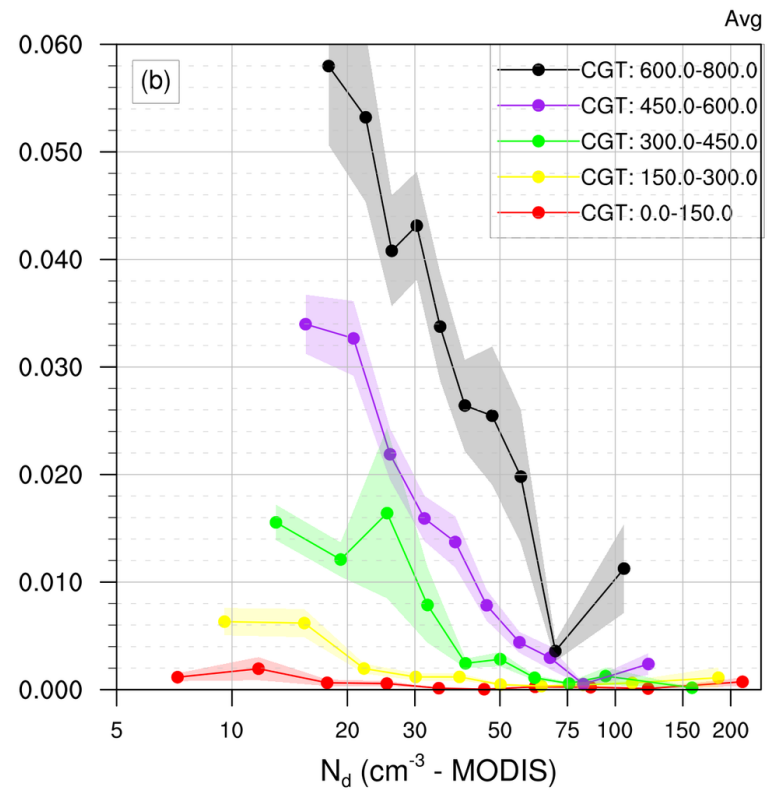
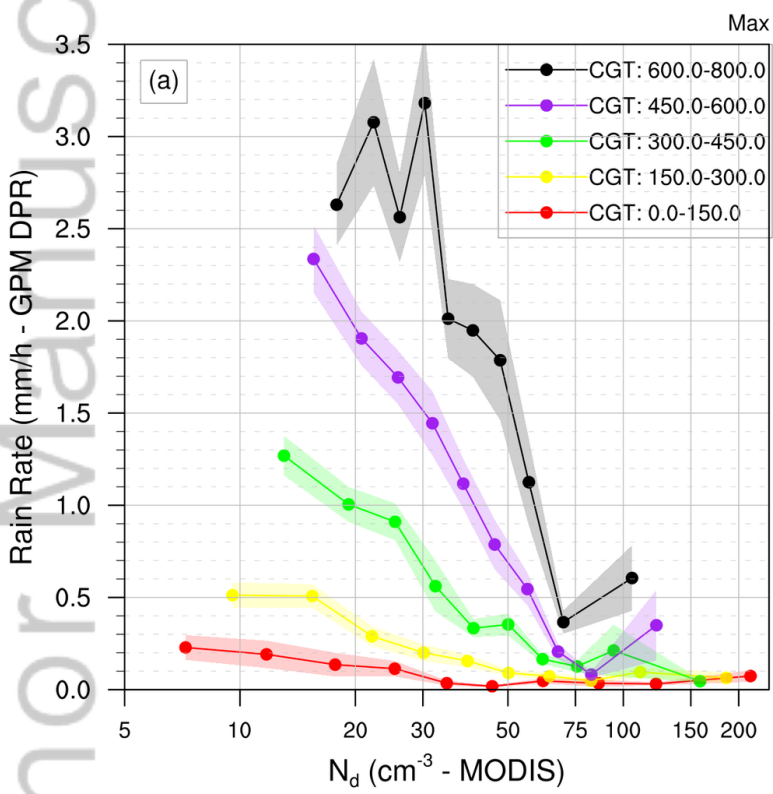
### References

Ackerman, A. S., Kirkpatrick, M. P., Stevens, D. E., & Toon, O. B. (2004). The impact of humidity above stratiform clouds on indirect aerosol climate forcing. *Nature*, 432(7020), 1014–1017. <https://doi.org/10.1038/nature03174>

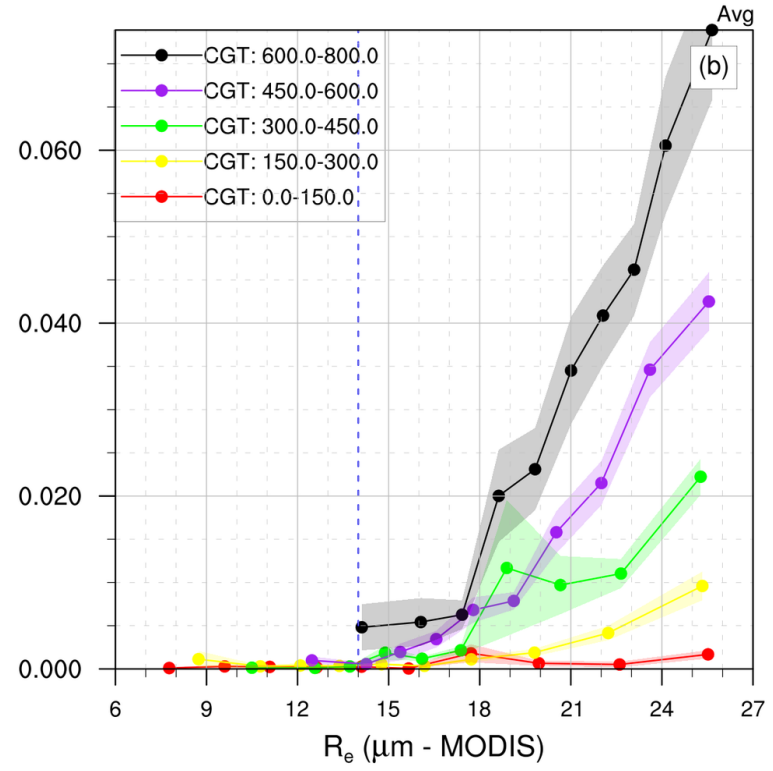
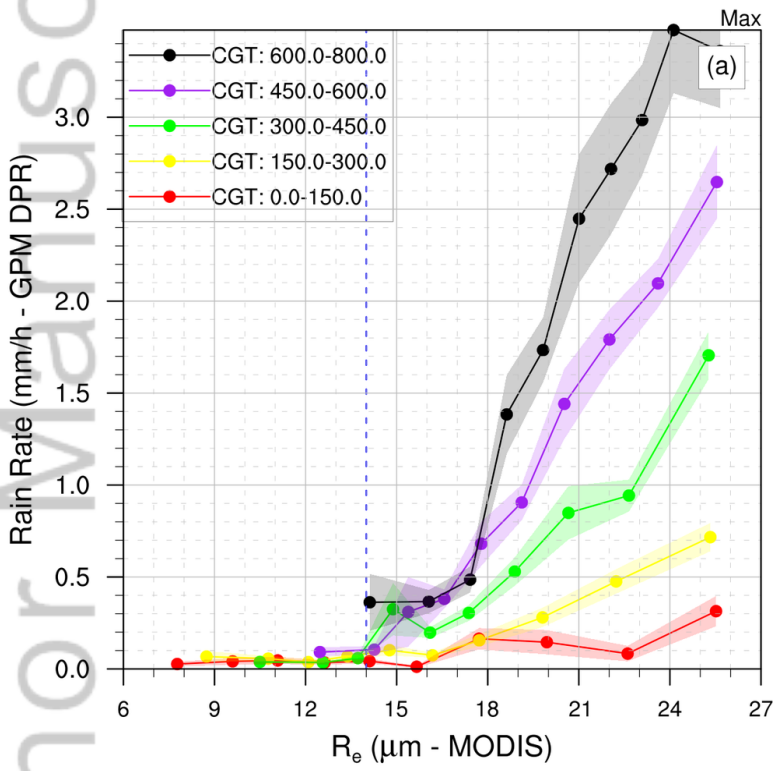
- Albrecht, B. A. (1989). Aerosols, Cloud Microphysics, and Fractional Cloudiness. *Science*, 245(4923), 1227–1230. <https://doi.org/10.1126/science.245.4923.1227>
- Boucher, O., & Quaas, J. (2013). Water vapour affects both rain and aerosol optical depth. *Nature Geoscience*, 6(1), 4–5. <https://doi.org/10.1038/ngeo1692>
- Boucher, O., Randall, D., Artaxo, P., Bretherton, C., Feingold, G., Forster, P., et al. (2013). Clouds and Aerosols. In Intergovernmental Panel on Climate Change (Ed.), *Climate Change 2013 - The Physical Science Basis* (Vol. 9781107057, pp. 571–658). Cambridge: Cambridge University Press. <https://doi.org/10.1017/CBO9781107415324.016>
- Chen, R., Wood, R., Li, Z., Ferraro, R., & Chang, F.-L. (2008). Studying the vertical variation of cloud droplet effective radius using ship and space-borne remote sensing data. *Journal of Geophysical Research*, 113(D8), D00A02. <https://doi.org/10.1029/2007JD009596>
- Dagan, G., Koren, I., & Altaratz, O. (2015). Competition between core and periphery-based processes in warm convective clouds – from invigoration to suppression. *Atmospheric Chemistry and Physics*, 15(5), 2749–2760. <https://doi.org/10.5194/acp-15-2749-2015>
- Dagan, Guy, Koren, I., Altaratz, O., & Heiblum, R. H. (2017). Time-dependent, non-monotonic response of warm convective cloud fields to changes in aerosol loading. *Atmospheric Chemistry and Physics*, 17(12), 7435–7444. <https://doi.org/10.5194/acp-17-7435-2017>
- Fan, J., Wang, Y., Rosenfeld, D., & Liu, X. (2016). Review of Aerosol–Cloud Interactions: Mechanisms, Significance, and Challenges. *Journal of the Atmospheric Sciences*, 73(11), 4221–4252. <https://doi.org/10.1175/JAS-D-16-0037.1>
- Freud, E., & Rosenfeld, D. (2012). Linear relation between convective cloud drop number concentration and depth for rain initiation. *Journal of Geophysical Research: Atmospheres*, 117(D2), D02207. <https://doi.org/10.1029/2011JD016457>
- Gryspeerd, E., Quaas, J., & Bellouin, N. (2016). Constraining the aerosol influence on cloud fraction. *Journal of Geophysical Research: Atmospheres*, 121(7), 3566–3583. <https://doi.org/10.1002/2015JD023744>
- Iguchi, T., Seto, S., Meneghini, R., Yoshida, N., Awaka, J., Le, M., et al. (2010). *GPM/DPR Level-2 Algorithm Theoretical Basis Document*. Greenbelt.
- Kapustin, V. N., Clarke, A. D., Shinozuka, Y., Howell, S., Brekhovskikh, V., Nakajima, T., & Higurashi, A. (2006). On the determination of a cloud condensation nuclei from satellite: Challenges and possibilities. *Journal of Geophysical Research*, 111(D4), D04202. <https://doi.org/10.1029/2004JD005527>
- Khan, S., Maggioni, V., & Kirstetter, P.-E. (2018). Investigating the Potential of Using Satellite-Based Precipitation Radars as Reference for Evaluating Multisatellite Merged Products. *Journal of Geophysical Research: Atmospheres*, 123(16), 8646–8660. <https://doi.org/10.1029/2018JD028584>
- Koren, I., Dagan, G., & Altaratz, O. (2014). From aerosol-limited to invigoration of warm convective clouds. *Science*, 344(6188), 1143–1146. <https://doi.org/10.1126/science.1252595>

- Koren, I., Altaratz, O., & Dagan, G. (2015). Aerosol effect on the mobility of cloud droplets. *Environmental Research Letters*, *10*(10), 104011. <https://doi.org/10.1088/1748-9326/10/10/104011>
- Malavelle, F. F., Haywood, J. M., Jones, A., Gettelman, A., Clarisse, L., Bauduin, S., et al. (2017). Strong constraints on aerosol–cloud interactions from volcanic eruptions. *Nature*, *546*(7659), 485–491. <https://doi.org/10.1038/nature22974>
- Nishant, N., & Sherwood, S. C. (2017). A cloud-resolving model study of aerosol–cloud correlation in a pristine maritime environment. *Geophysical Research Letters*, *44*(11), 5774–5781. <https://doi.org/10.1002/2017GL073267>
- Pinsky, M. B., & Khain, A. P. (2002). Effects of in-cloud nucleation and turbulence on droplet spectrum formation in cumulus clouds. *Quarterly Journal of the Royal Meteorological Society*, *128*(580), 501–533. <https://doi.org/10.1256/003590002321042072>
- Platnick, S., Ackerman, A. S., King, M. D., Meyer, K., W.P., M., Holz, R. E., et al. (2015). MODIS atmosphere L2 cloud product (06\_L2). *NASA MODIS Adaptive Processing System*. NASA MODIS Adaptive Processing System, Goddard Space Flight Center. [https://doi.org/http://dx.doi.org/10.5067/MODIS/MOD06\\_L2.006](https://doi.org/http://dx.doi.org/10.5067/MODIS/MOD06_L2.006)
- Quan, J., Jiang, C., Xin, J., Zhao, X., Jia, X., Liu, Q., et al. (2018). Evaluation of satellite aerosol retrievals with in situ aircraft and ground measurements: Contribution of relative humidity. *Atmospheric Research*, *212*, 1–5. <https://doi.org/10.1016/j.atmosres.2018.04.024>
- Rosenfeld, D., Zheng, Y., Hashimshoni, E., Pöhlker, M. L., Jefferson, A., Pöhlker, C., et al. (2016). Satellite retrieval of cloud condensation nuclei concentrations by using clouds as CCN chambers. *Proceedings of the National Academy of Sciences*, *113*(21), 5828–5834. <https://doi.org/10.1073/pnas.1514044113>
- Rosenfeld, D., Zhu, Y., Wang, M., Zheng, Y., Goren, T., & Yu, S. (2019). Aerosol-driven droplet concentrations dominate coverage and water of oceanic low-level clouds. *Science*, *363*(6427), eaav0566. <https://doi.org/10.1126/science.aav0566>
- Stephens, G., & Slingo, T. (1992). An air-conditioned greenhouse. *Nature*, *358*(6385), 369–370. <https://doi.org/10.1038/358369a0>
- Stier, P. (2016). Limitations of passive remote sensing to constrain global cloud condensation nuclei. *Atmospheric Chemistry and Physics*, *16*(10), 6595–6607. <https://doi.org/10.5194/acp-16-6595-2016>
- Tao, W.-K., Chen, J.-P., Li, Z., Wang, C., & Zhang, C. (2012). Impact of aerosols on convective clouds and precipitation. *Reviews of Geophysics*, *50*(2). <https://doi.org/10.1029/2011RG000369>
- Toll, V., Christensen, M., Quaas, J., & Bellouin, N. (2019). Weak average liquid–cloud–water response to anthropogenic aerosols. *Nature*, *572*(7767), 51–55. <https://doi.org/10.1038/s41586-019-1423-9>
- Twomey, S. (1977). The Influence of Pollution on the Shortwave Albedo of Clouds. *Journal of the Atmospheric Sciences*, *34*(7), 1149–1152. [https://doi.org/10.1175/1520-0469\(1977\)034<1149:TIOPOT>2.0.CO;2](https://doi.org/10.1175/1520-0469(1977)034<1149:TIOPOT>2.0.CO;2)

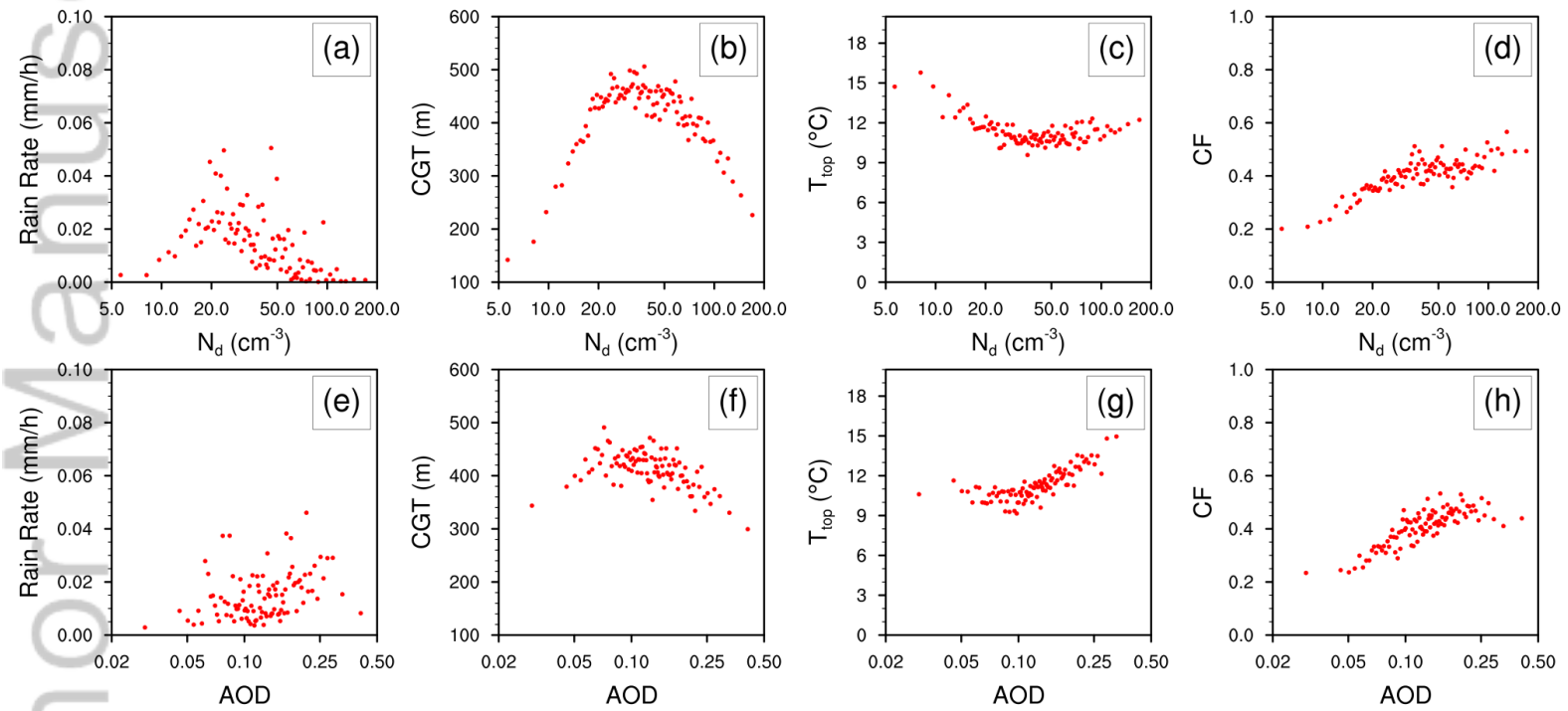
- vanZanten, M. C., Stevens, B., Vali, G., & Lenschow, D. H. (2005). Observations of Drizzle in Nocturnal Marine Stratocumulus. *Journal of the Atmospheric Sciences*, *62*(1), 88–106. <https://doi.org/10.1175/JAS-3355.1>
- Wang, M., Ghan, S., Liu, X., L'Ecuyer, T. S., Zhang, K., Morrison, H., et al. (2012). Constraining cloud lifetime effects of aerosols using A-Train satellite observations. *Geophysical Research Letters*, *39*(15), L15709. <https://doi.org/10.1029/2012GL052204>
- Yang, Y., Russell, L. M., Lou, S., Liu, Y., Singh, B., & Ghan, S. J. (2016). Rain-aerosol relationships influenced by wind speed. *Geophysical Research Letters*, *43*(5), 2267–2274. <https://doi.org/10.1002/2016GL067770>
- Zhu, Y., Rosenfeld, D., & Li, Z. (2018). Under What Conditions Can We Trust Retrieved Cloud Drop Concentrations in Broken Marine Stratocumulus? *Journal of Geophysical Research: Atmospheres*, *123*(16), 8754–8767. <https://doi.org/10.1029/2017JD028083>



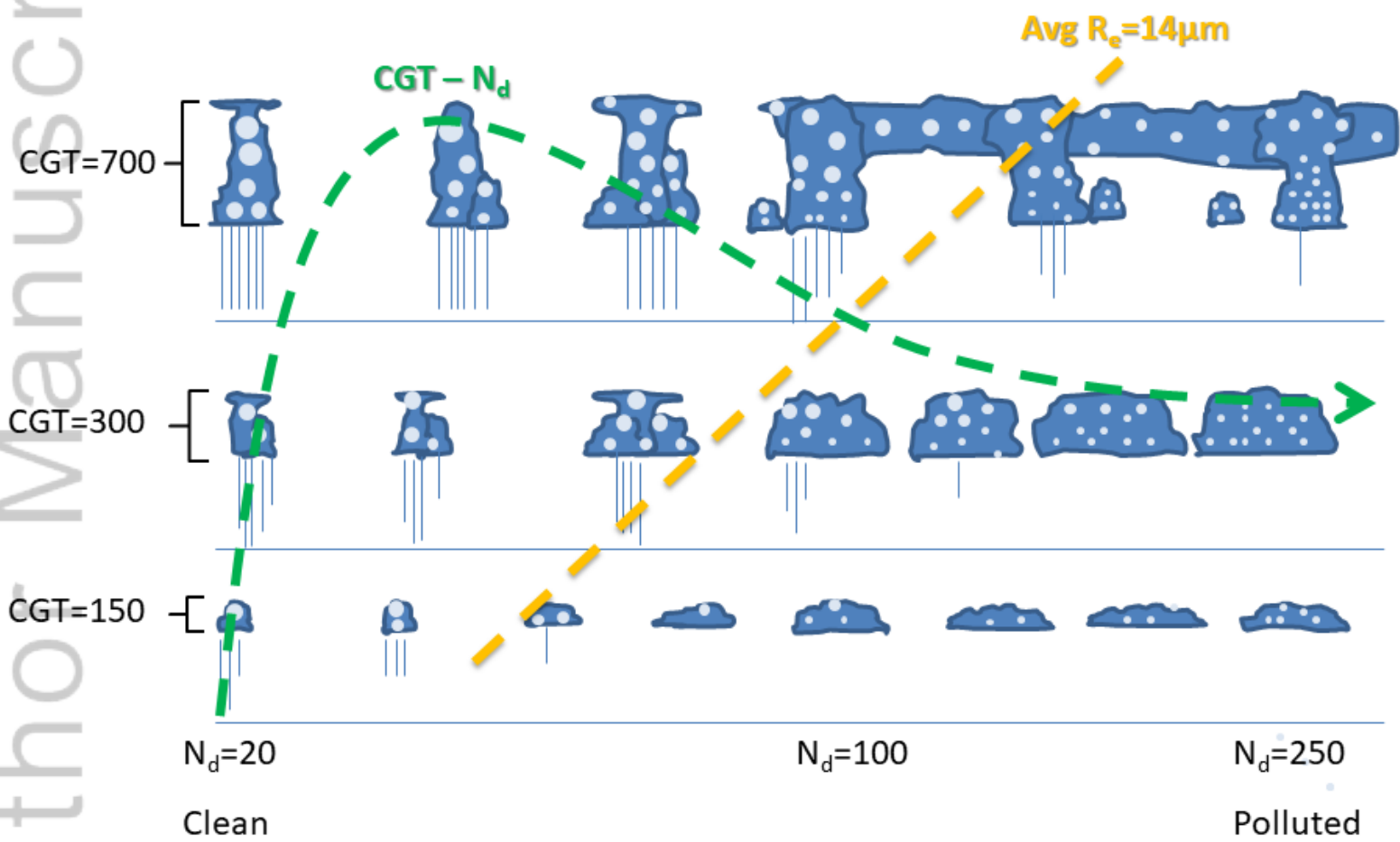
2019GL086207-f01-z-.png



2019GL086207-f02-z-.png



2019GL086207-f03-z-.png



2019GL086207-f04-z-.png